Near-wall damping in model predictions of separated flows

By Martin Skote[*] and Stefan Wallin[†]

Data from the near-wall region of an attached and a separated turbulent boundary layer are used for the development of near-wall damping functions utilized in turbulence modelling. The model considered is an explicit algebraic Reynolds stress model. The data are taken from two direct numerical simulations. The turbulent boundary layer equation is analyzed in order to extend the validity of existing wall damping functions to turbulent boundary layers under severe adverse pressure gradients.

1. Introduction

Two turbulent boundary layers subject to adverse pressure gradients (APG) were investigated through direct numerical simulation (DNS) by Skote & Henningson (2000). The two APG distributions are quite similar, but the influence of the APG on the flow is strong, creating two very different boundary layer flows. One is everywhere attached (APG1), and the other is separated for a long streamwise section (SEP).

The data are here used for assessing the near-wall scaling of wall damping functions used in turbulence modelling. The particular model studied is the fully self-consistent explicit algebraic Reynolds stress model (EARSM) developed by Wallin & Johansson (2000), which can, in contrast to standard eddy-viscosity two-equation models, be successfully damped in the vicinity of a wall in zero pressure-gradient boundary layers by employing the standard van Driest damping function.

A relevant velocity scale is crucial for the correct behaviour of wall damping functions used in turbulence models. For a zero pressure gradient (ZPG) boundary layer, the damping functions and boundary conditions in the logarithmic layer are based on a theory in which the friction velocity,

$$u_\tau \equiv \sqrt{\nu \left.\frac{\partial u}{\partial y}\right|_{y=0}}, \tag{1}$$

is used as a velocity scale. However, in the case of a boundary layer under an APG, u_τ is not the relevant velocity scale, especially not for a strong APG

[*]Department of Mechanics, KTH, SE-100 44 Stockholm, Sweden
[†]Aeronautical Research Institute of Sweden,Box 11021, SE-161 11 Bromma, Sweden

and low Reynolds number. In the case of separation this is clear since u_τ becomes zero. Wall damping functions based on $y^+ \equiv yu_\tau/\nu$ are, thus, not appropriate. Other possibilities than y^+ that are used in near-wall damping functions are $Re_y \equiv \sqrt{K}y/\nu$ or the turbulent Reynolds number $Re_t \equiv K^2/\nu\varepsilon$ (see e.g. Wilcox (1993)). These alternatives do not have the singularity caused by that u_τ becomes zero.

The scaling laws developed in many previous studies have been in a form not suitable for turbulence models. Instead, the aim for the scaling of the velocity profile has often been to create a tool for different prediction methods based on the simplified turbulent boundary-layer equations (TBLE). The motivation for the thorough scaling analysis performed here is that the turbulence modelling can be improved if the correct scaling is used. However, the scalings are entirely motivated by the TBLE itself, i.e. turbulence modelling is disregarded when performing the scaling analysis of the TBLE.

Many of the earlier theoretical analyses were not performed with the same objectives as we have today. Hence, the results, though interesting in many aspects, perhaps lack a natural potential for direct application to the final goal — to calculate and predict a turbulent boundary layer flow.

Some basic ideas concerning the velocity scale in the inner part of the turbulent boundary layer under an APG are presented in section 2. It is shown that the total shear stress varies linearly in a turbulent boundary layer under an APG, if the Reynolds number is not large compared with the APG. The linear behaviour leads to a velocity scale dependent on the normal coordinate, replacing the friction velocity as a velocity scale.

The new velocity scale is used in the wall damping of the EARSM model in section 3. Comparison with the damping based on Re_y proposed by Wallin & Johansson (2000) is made, and an example of the performance of EARSM with the improved damping is given.

2. Scalings in the near-wall region

When neglecting the non-linear, advective terms in the equations describing the mean flow, the equation governing the inner part of the boundary layer is obtained. This equation can, when using the inner length and velocity scales ν/u_τ and u_τ be written,

$$0 = -\frac{\nu}{u_\tau^3}\frac{1}{\rho}\frac{dP}{dx} + \frac{d^2u^+}{dy^{+2}} - \frac{d}{dy^+}\langle u'v'\rangle^+, \tag{2}$$

where $\langle u'v'\rangle$ is the Reynolds shear stress. If the term involving the pressure gradient is smaller than the other terms, the equation reduces to the equation governing the inner part of a ZPG boundary layer. However, for strong APG cases at finite Reynolds numbers, this term cannot be neglected. Equation (2) can be integrated to give an expression for the total shear stress,

$$\tau^+ \equiv \frac{du^+}{dy^+} - \langle u'v'\rangle^+ = 1 + \frac{\nu}{u_\tau^3}\frac{1}{\rho}\frac{dP}{dx}y^+. \tag{3}$$

For a zero pressure gradient case, equation (3) predicts a constant shear stress of unity. For an APG case with a freestream distribution of the form $U \sim x^m$, the last term in equation (3) can be shown (Skote *et al.* 1998) to decrease with increasing Reynolds number.

When considering a strong APG or separation, A singularity occurs when u_τ becomes zero, which can be avoided by introducing the velocity scale,

$$u_p \equiv \left(\nu \frac{1}{\rho} \frac{dP}{dx}\right)^{1/3}. \tag{4}$$

First equation (3) is formulated as

$$\tau^+ = 1 + \left(\frac{u_p}{u_\tau}\right)^3 y^+. \tag{5}$$

The velocity scale u_p has to be used instead of u_τ if the last term in equation (5) becomes very large which happens if $u_\tau \ll u_p$, i.e. the boundary layer is close to separation. This was noted by Stratford (1959), Townsend (1961) and Tennekes & Lumley (1972). By multiplying equation (5) by $(u_p/u_\tau)^2$, the following expression for $\tau^p \equiv \tau/u_p^2$ as a function of $y^p \equiv y u_p/\nu$ is obtained,

$$\tau^p = y^p + \left(\frac{u_\tau}{u_p}\right)^2. \tag{6}$$

Equation (6) has the asymptotic form $\tau^p = y^p$ when separation is approached. Thus, in this rescaled form, the singularity is avoided.

For the ZPG case, the scaling of the total shear stress with u_τ gives a self-similar profile ($\tau^+ = 1$). From equations (5) and (6) it is observed that neither u_τ nor u_p as velocity scale results in a self-similar expression. However, equation (3) can be formulated as

$$\tau^* \equiv \frac{1}{u_*^2}\left(\nu \frac{\partial u}{\partial y} - \langle u'v' \rangle\right) = 1, \tag{7}$$

where u_* is a velocity scale that depends on y and can be expressed in either plus or pressure gradient units,

$$u_*^2 = u_\tau^2 + \frac{u_p^3}{u_\tau} y^+ = u_\tau^2 + u_p^2 y^p. \tag{8}$$

Thus, by scaling the total shear stress with u_*, a self-similar expression is obtained ($\tau^* = 1$). The velocity scale u_* reduces to u_τ if u_p becomes zero, i.e. for a ZPG boundary layer. If instead u_τ becomes zero, i.e. a boundary layer at separation, the velocity scales becomes $u_* = u_p\sqrt{y^p}$.

For the special case with $u_\tau = 0$, the velocity scale u_* is zero at the wall. This is natural since the velocity gradient is zero at the wall. Previous investigators of the mixing length theory have also observed the importance of u_*, see Granville (1989) for references.

From u_* it is possible to define the length scale ν/u_*, and thus a normalized normal coordinate, $y^* \equiv yu_*/\nu$ which can be written,

$$y^* = \sqrt{(y^+)^2 + (y^p)^3}. \tag{9}$$

If a separated flow is considered, the definition of u_τ has to be reconsidered. In the separated region, $\frac{\partial u}{\partial y}$ is negative. Thus, the definition of u_τ in equation (1) involves a square root of a negative number. Instead, the definition will be changed so that the square root will be taken of a positive number.

To proceed with the analysis of the equations, the definition of the friction velocity will have to be changed to

$$u_\tau \equiv \sqrt{-\nu \frac{\partial u}{\partial y}\bigg|_{y=0}}. \tag{10}$$

In the case of a separated flow, the change of sign of the wall shear stress leads to a u_* as,

$$u_*^2 = -u_\tau^2 + \frac{u_p^3}{u_\tau} y^+ \tag{11}$$

The velocity scale u_*^2 is in the case of separation negative for $y^+ < (u_\tau/u_p)^3$, because the shear stress is negative at those values of y^+. Hence, the length scale ν/u_* has to be used with a restriction to positive values of u_*^2. This leads to a y^* of the form,

$$y^* = \sqrt{\max\{0, -(y^+)^2 + (y^p)^3\}}. \tag{12}$$

3. Evaluation of turbulence models

The aim with this part of the work is to investigate how predictions of turbulent boundary layer flow is affected by the complication of a severe APG and separation. In the near-wall part of the flow, turbulence models often utilize damping functions. Their purpose is to damp various physical quantities in the neighborhood of a wall. One important step towards better model predictions in APG flows is the refinement of the damping functions.

The results regarding the near-wall flow reported in Skote & Henningson (1999) and Skote & Henningson (2000) can be utilized in turbulence model predictions directly as, so called, wall-function boundary conditions. Here we are instead interested in resolving the turbulent boundary layer all the way to the wall and thus the wall damping functions become important.

A short description of the DNS and the turbulent boundary layer flows is given in section 3.1. The specific turbulence model used in the present work (EARSM), is described in section 3.2. A priori tests done with DNS data from both simulations are presented in section 3.3, together with the development of damping functions. The relation between two length scales used in the near-wall damping is analyzed in section 3.4. In section 3.5 some examples of the performance of the EARSM model is shown, using the data from DNS.

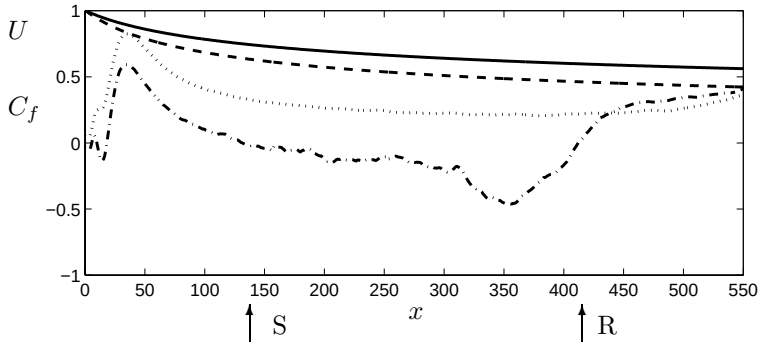

FIGURE 1. APG1: — U; $\cdots$ $C_f \times 100$. SEP: - - U; $-\cdot-$ $C_f \times 100$. S and R denote the points of separation and reattachment respectively for SEP.

	APG1	SEP		
	$x = 150$	$x = 300$	$x = 412$	$x = 450$
U	0.73	0.51	0.46	0.45
u_τ	0.0287	0.0165	0.0024	0.0166
u_p	0.0117	0.0086	0.0074	0.0071

TABLE 1. Some parameters of the turbulent boundary layers at different downstream positions.

3.1. *Description of the test cases*

The data from the two turbulent boundary layers considered in the present work were taken from a DNS performed by Skote & Henningson (2000).

The freestream velocity (U) for the two simulations, APG1 and SEP, are shown in figure 1, together with the skin friction (C_f). As seen from the figure, a small change in the freestream velocity has a great impact on the skin friction. In APG1, the boundary layer is subject to a strong APG, but is everywhere attached. In SEP the boundary layer is separated for a large portion of the computational domain.

The simulations start with a laminar boundary layer at the inflow ($x = 0$) which is triggered to transition by a random volume force near the wall. The flow is fully turbulent at $x = 100$.

The downstream coordinate x is scaled with the displacement thickness (δ^*) at the starting position of the simulation ($x = 0$), where the flow is laminar and $Re_{\delta^*} = 400$.

Table 3.1 serves as a comparison of the two cases at the downstream positions investigated in the present work.

3.2. *The basic models*

In two-dimensional mean flows, the fully self-consistent explicit algebraic Reynolds stress model may be formulated based on any (quasi-)linear pressure-strain model (see Wallin & Johansson (2000) and Girimaji (1997) for details). Neglecting the advection and diffusion of the Reynolds stress anisotropy $a_{ij} \equiv \langle u_i' u_j' \rangle / K - 2\delta_{ij}/3$ results in an implicit and non-linear relation

$$\begin{aligned} 0 = & \left(A_3 + A_4 \frac{\mathcal{P}}{\varepsilon} \right) a_{ij} + A_1 S_{ij} - (a_{ik}\Omega_{kj} - \Omega_{ik}a_{kj}) \\ & + A_2 \left(a_{ik}S_{kj} + S_{ik}a_{kj} - \frac{2}{3} a_{kl}S_{lk}\delta_{ij} \right). \end{aligned} \tag{13}$$

where $S_{ij} \equiv \tau/2(U_{i,j} + U_{j,i})$ and $\Omega_{ij} \equiv \tau/2(U_{i,j} - U_{j,i})$ are the symmetric and antisymmetric parts of the velocity gradient tensor normalized by the turbulent time scale $\tau \equiv K/\varepsilon$.

In a two-dimensional mean flow the solution for the anisotropy becomes

$$\begin{aligned} a_{12} &= \beta_1 S_{12} + 2\beta_4 S_{11}\Omega_{12} \\ a_{11} &= \beta_1 S_{11} + \beta_2 \left(S_{11}^2 + S_{12}^2 - \frac{1}{3} II_S \right) - 2\beta_4 S_{12}\Omega_{12} \\ a_{22} &= -\beta_1 S_{11} + \beta_2 \left(S_{11}^2 + S_{12}^2 - \frac{1}{3} II_S \right) + 2\beta_4 S_{12}\Omega_{12} \\ a_{33} &= \beta_2 \left(-\frac{1}{3} II_S \right) \end{aligned} \tag{14}$$

where the β coefficients are functions of the flow invariants $II_S \equiv S_{ij}S_{ji}$ and $II_\Omega \equiv \Omega_{ij}\Omega_{ji}$ and the model coefficients A_{1-4} in equation (13). Two different EARSMs will be considered; the "W&J" model, Wallin & Johansson (2000), based on a recalibrated LRR (Launder *et al.* 1975) pressure-strain rate model and the "Gir" model, Girimaji (1997), based on the linearized SSG (Speziale *et al.* 1991) pressure-strain rate model. The corresponding A_{1-4} coefficients are given in table 3.2. The "W&J" model results in that the β_2 coefficient is zero and as a consequence $a_{33} = 0$.

In two-dimensional mean flows the β coefficients are given by

$$\beta_1 = -\frac{A_1 N}{Q}, \quad \beta_2 = 2\frac{A_1 A_2}{Q}, \quad \beta_4 = -\frac{A_1}{Q}, \tag{15}$$

where the denominator is

$$Q = N^2 - 2II_\Omega - \frac{2}{3} A_2^2 II_S. \tag{16}$$

	A_1	A_2	A_3	A_4
W&J (Recalibrated LRR)	1.20	0	1.80	2.25
Gir (Linearized SSG)	1.22	0.47	0.88	2.37

TABLE 2. The values of the A-coefficients for different quasi-linear pressure-strain models.

N is given by

$$N = \begin{cases} \frac{A_3}{3} + \left(P_1 + \sqrt{P_2}\right)^{1/3} + \text{sign}\left(P_1 - \sqrt{P_2}\right) \mid P_1 - \sqrt{P_2} \mid^{1/3}, & P_2 \geq 0 \\ \frac{A_3}{3} + 2\left(P_1^2 - P_2\right)^{1/6} \cos\left(\frac{1}{3}\arccos\left(\frac{P_1}{\sqrt{P_1^2 - P_2}}\right)\right), & P_2 < 0 \end{cases} \tag{17}$$

where

$$\begin{aligned} P_1 &= \left(\frac{{A_3}^2}{27} + \left(\frac{A_1 A_4}{6} - \frac{2}{9}{A_2}^2\right) II_S - \frac{2}{3} II_\Omega\right) A_3 \\ P_2 &= P_1^2 - \left(\frac{{A_3}^2}{9} + \left(\frac{A_1 A_4}{3} + \frac{2}{9}{A_2}^2\right) II_S + \frac{2}{3} II_\Omega\right)^3 . \end{aligned} \tag{18}$$

3.3. *Near-wall treatments*

In the model proposed by Wallin & Johansson (2000) the correct near-wall behaviour for zero pressure-gradient boundary layers was obtained by modifying the β coefficients using a damping function of the van Driest type. The original form was based on y^+, but an alternative suggestion of the damping function was based on $y^T = y^T(Re_y)$ in order of avoiding the singularity in separated flows. The function y^T was constructed to be similar to y^+ for $y^+ < 100$ in zero pressure-gradient boundary layers. In this section the different near-wall scalings will be assessed by comparing model predictions using y^+, y^T as well as y^*.

In a two-dimensional mean flow the near-wall corrections for the "W&J" model reads

$$\begin{aligned} \beta_1 &= f_1 \beta_1^* \\ \beta_2 &= f_1^2 \beta_2^* + (1 - f_1^2) \frac{3B_2 - 4}{\max\left(II_S, II_S^{eq}\right)} \\ \beta_4 &= f_1^2 \beta_4^* - (1 - f_1^2) \frac{B_2}{2\max\left(II_S, II_S^{eq}\right)} \end{aligned} \tag{19}$$

where β_1^*, β_2^* and β_4^* are the "high-Re" uncorrected coefficients given by (15) and the damping function

$$f_1 = 1 - \exp(-y^+/A^+) \tag{20}$$

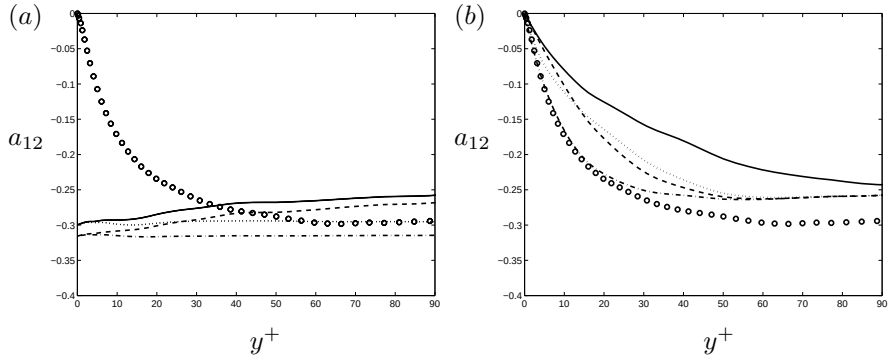

FIGURE 2. APG1 at $x = 150$: (a) ∘ DNS; — non-damped "W&J"; ⋯ non-damped "W&J" with $\beta_4 = 0$; - - non-damped "Gir"; -·- non-damped "Gir" with $\beta_4 = 0$. (b) ∘ DNS. Damped "W&J" with the scaled coordinate in f_1 as — y^+; - - y^*; ⋯ y^T. -·- damped "W&J" with y^+ and $A^+ = 11$.

and the model coefficients

$$\Pi_S^{eq} = 5.74 \qquad B_2 = 1.8 \tag{21}$$

For the damped expressions the turbulent time scale used for normalizing the velocity gradient tensors must be limited by the viscous scale, such as

$$\tau \equiv \max\left(\frac{K}{\varepsilon}, C_\tau\sqrt{\frac{\nu}{\varepsilon}}\right) \tag{22}$$

where $C_\tau = 6.0$ is used.

For the Girimaji (1997) model based on the linearized SSG model no near-wall corrections are present and, thus, only the non-damped "Gir" model will be tested.

3.3.1. *APG1*

In this section different modelling assumptions are tested by using DNS data from the attached APG boundary layer (APG1). The anisotropies are calculated from equation (14) with S_{ij} and Ω_{ij} computed from DNS data. The resulting anisotropies are then compared with those taken directly from the DNS.

The shear anisotropy a_{12} is plotted for one streamwise position ($x = 150$) in figure 2. The behaviour is approximately the same at all streamwise positions for APG1. The anisotropy taken directly from DNS data is shown with circles. The non-damped models "W&J" and "Gir" are shown in figure 2a. Both models overpredict the asymptotic value at large y^+, which is around -0.3 in the DNS data. The failure to correctly predict the asymptotic value is due to that the basic, undamped, models do not correctly respond to the pressure

gradient. The error enters mainly through the non-linear term in equation (14a) and the best result is actually obtained with $\beta_4 = 0$ for the "W&J" model, as shown in figure 2a with the dotted line. Setting $\beta_4 = 0$ should, however, not be considered as an alternative for improving the model behaviour since the β_4 term results from a formal approximation of the basic Reynolds stress transport model. Moreover, the β_4 term gives important contributions for the normal anisotropy components.

Near the wall, damping with f_1 becomes important. The a_{12} profiles from the damped "W&J" model are shown in figure 2b. The standard van Driest damping, equation (20), with the standard value of $A^+ = 26$, does not give the correct near-wall damping (the solid line in figure 2b). Thus, the standard van Driest damping, which gives a good agreement for a ZPG boundary layer, must be improved in order to give reasonable results for an APG flow. The most straight forward correction is to change the value of A^+ in equation (20).

The damped profiles give very different results depending on the value of A^+. The value of $A^+ = 11$ was observed to give the best agreement with the DNS data, (the dash-dotted profile in figure 2b), and by setting $\beta_4 = 0$ almost perfect agreement with DNS was obtained.

There are many relations between A^+ and the ratio u_p/u_τ proposed in the literature. Kays (1971) proposed the relation,

$$A^+ = \frac{26}{1 + 30.18\left(\frac{u_p}{u_\tau}\right)^3}, \tag{23}$$

which gives a value of $A^+ = 8.6$ for APG1. This value is far from the standard value of 26, but does not agree with the best fitted value of 11 for APG1. In the experimental work of Nagano *et al.* (1992) however, the formula (23) gave good predictions. Cebeci (1970) proposed the relation,

$$A^+ = \frac{26}{\sqrt{1 + 11.8\left(\frac{u_p}{u_\tau}\right)^3}}, \tag{24}$$

which gives a value of $A^+ = 19.4$ for APG1. This value is closer to 26, but far from the value of 11. Granville (1989) proposed a relation which is similar to equation (24), with a factor of 12.6 instead of 11.8, which gives very similar values of A^+ as the relation (24).

A list of other relations is included in the work of Granville (1989). However, the above relations were derived from a mixing length hypothesis, which states that the Reynolds shear stress is linked to the velocity gradient through,

$$-\langle u'v'\rangle^+ = (l^+)^2 \left(\frac{du^+}{dy^+}\right)^2, \tag{25}$$

with

$$l^+ = \kappa y^+ f_1 \qquad \text{or} \qquad l^+ = \kappa y^* f_1, \tag{26}$$

and f_1 as in equation (20). The coordinate y^* is given in equation (9). The second form of l^+ above (26b) was, among others, used by Granville (1989). However, he let a factor α reduce the influence of the pressure gradient,

$$y^* = \sqrt{(y^+)^2 + \alpha \left(\frac{u_p}{u_\tau}\right)^3 (y^+)^3} \tag{27}$$

There is some discrepancy regarding the value of α in the literature. Perry *et al.* (1966) proposed a varying α from 0.65 to 0.9, while Granville (1989) specified 0.9 and McDonald (1969) 0.7. When Skåre & Krogstad (1994) investigated the formula (26b), they had to change the value of κ from 0.41 to 0.78 to fit with experimental data through the logarithmic layer. In the present investigation, the influence of α and κ will not be considered important, since the goal is not to create a mixing length theory, but to use the best damping function for the EARSM model.

In the EARSM model, the relation between the Reynolds shear stress and the velocity gradient is more complicated than equation (25), and an analysis is not as straightforward. The damping with f_1 as in equation (20), which was developed from the mixing-length theory, has proved to work well for the EARSM model for channel flow and ZPG boundary layer flow. For the APG boundary layer flow however, the damping of both the mixing-length theory, equation (25), and the EARSM has to be developed. To further investigate this idea for the EARSM model, where no mixing length exists, the viscous scaling of the normal coordinate in f_1 is substituted with the y^*, defined in section 2.

Arguing that u_τ no longer is the relevant velocity scale, the scaled normal coordinate y^+ in equation (20) may be changed to y^*. A different length scale was proposed by Wallin & Johansson (2000), and their scaled normal coordinate y^T, is defined as,

$$y^T = C_{y1}\sqrt{Re_y} + C_{y2}Re_y^2, \tag{28}$$

where $Re_y = \sqrt{K}y/\nu$, $C_{y1} = 2.4$ and $C_{y2} = 0.003$.

Thus, the damping function f_1 can be expressed as,

$$f_1 = 1 - \exp(-y^*/A^+), \tag{29}$$

or

$$f_1 = 1 - \exp(-y^T/A^+). \tag{30}$$

The formulation of f_1 as in equation (29) was actually used for the mixing length damping by Cebeci & Smith (1968).

A third possibility would be to use y^p. However, to change from y^+ to y^p cannot give any improvement since they are linearly dependent of each other. Thus, the same f_1 profile can be obtained by using y^+ or y^p if the constant A^+ is adjusted.

In figure 2b, the "W&J" model damped with f_1 based on the scaled normal coordinates y^* and y^T are shown. They work almost equally well and the original value of $A^+ = 26$ was kept.

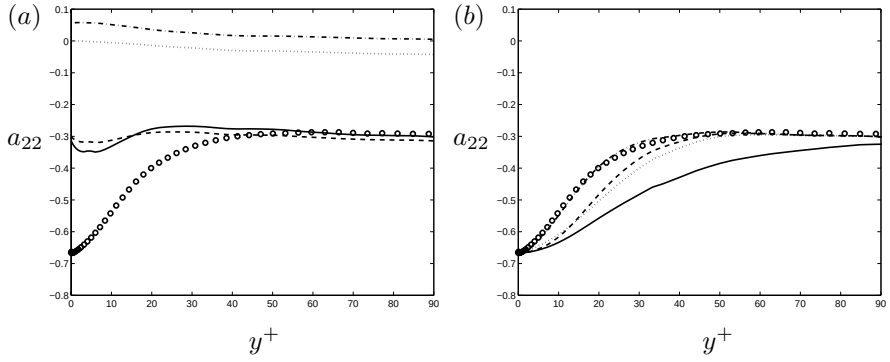

FIGURE 3. APG1 at $x = 150$: (a) ∘ DNS; — non-damped "W&J"; ⋯ non-damped "W&J" with $\beta_4 = 0$; - - non-damped "Gir"; -·- non-damped "Gir" with $\beta_4 = 0$. (b) ∘ DNS. Damped "W&J" with the scaled coordinate in f_1 as — y^+; - - y^*; ⋯ y^T. -·- damped "W&J" with y^+ and $A^+ = 11$.

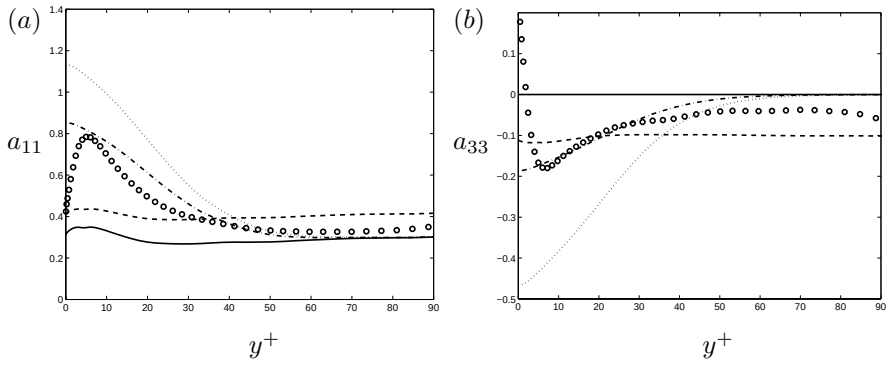

FIGURE 4. APG1 at $x = 150$. (a) a_{11}. (b) a_{33}. ∘ DNS; — non-damped "W&J"; - - non-damped "Gir"; ⋯ damped "W&J" with the scaled coordinate in f_1 as y^T; -·- same as the previous profile but with B_2=1.52.

Since the dependency of A^+ on the pressure gradient and Reynolds number (u_p/u_τ) seems difficult to describe correctly, the rescaled functions (29) and (30) are good alternatives for achieving proper damping in APG flows.

The good results obtained with $\beta_4 = 0$ for a_{12} is not consistent with the results for a_{22}, shown in figure 3. Here, the β_4 coefficient is important to get agreement with DNS data for large values of y^+. Both the "W&J" and "Gir" models predict the asymptotic value of a_{22} well. The profiles from the damped "W&J" model are shown in figure 3b. The alternative length scales y^* and y^T with $A^+ = 26$ are also here very similar and give clear improvements compared

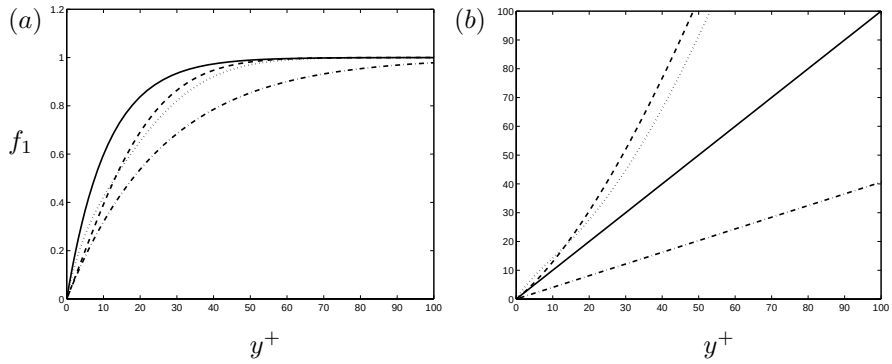

FIGURE 5. APG1 at $x = 150$: (a) f_1 using — y^+ and $A^+ = 11$; - - y^* and $A^+ = 26$; $\cdots$ y^T and $A^+ = 26$; -·- y^+ and $A^+ = 26$. (b) — y^+; - - y^*; $\cdots$ y^T; -·- y^p.

to the y^+ scaling. The best fit is obtained by using y^+ with $A^+ = 11$ also in this case.

The anisotropies a_{11} and a_{33} are shown in figure 4a and b. For a_{11} the "W&J" model gives better agreement with DNS data at large y^+ than the "Gir" model. The damped "W&J" model gives profiles with the same trend as for a_{12} and a_{22}, i.e. the alternative length scales y^* and y^T with $A^+ = 26$ work equally well as y^+ with $A^+ = 11$. Only the y^T damped profile is shown (dotted line) in figure 4a . For a_{33} (figure 4b), the non-damped "W&J" model predicts a value of zero. However, the "Gir" model does not give a better prediction even though it is non-zero. The damped "W&J" model results in a profile (dotted line) that gives a poor agreement with DNS data close to the wall. The wall values of a_{11} and a_{33} are controlled by the B_2 coefficient, and by modifying that to 1.52 almost perfect agreement is obtained (see figure 4). The original value $B_2 = 1.8$ was calibrated from channel flow and the different value obtained for this case indicates that there are a pressure-gradient dependency in B_2.

The damping functions are shown in figure 5a. The function based on y^+ with the optimal value of $A^+ = 11$, and the functions based on y^* and y^T reach unity after approximately $y^+ = 40$. Thus, the damping has no effect for y^+ over approximately 40. The change from the original shape (with y^+ and $A^+ = 26$) is large. In figure 5b the scaled normal coordinates are shown as a function of y^+. From figure 5b it is noted that y^p is proportional to y^+, which is obvious since both u_τ and u_p are independent on y.

In conclusion, the change from y^+ to y^* or y^T, is recommended in favour of keeping the y^+ scaling where the value of A^+ has to be changed for different APG layers. A specific value has to be obtained for each APG and also for each downstream position if the range of Reynolds numbers is large. The value of $A^+ = 11$ is only valid for the APG1 case presented here. For a less severe

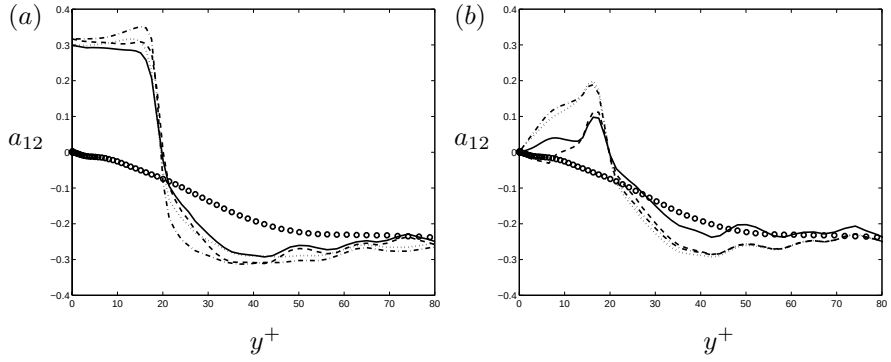

FIGURE 6. SEP at $x = 300$: (a) $\circ$ DNS; — non-damped "W&J" $\cdots$ non-damped "W&J" with $\beta_4 = 0$; - - non-damped "Gir"; -·- non-damped "Gir" with $\beta_4 = 0$. (b) $\circ$ DNS. Damped "W&J" with the scaled coordinate in f_1 as — y^+; - - y^*; $\cdots$ y^T. -·- damped "W&J" with y^+ and $A^+ = 11$.

APG, the value of A^+ has to be increased, whereas the scaling with y^* or y^T can be kept intact. In the extreme case of $u_\tau = 0$, the formulation with y^* or y^T is still valid, whereas the y^+ formulation encounters a singularity, no matter what value of A^+ being used. The extreme case of ZPG is the limit where the value of A^+ is 26 in y^+ formulation and the formulation with y^* is equivalent with the y^+ damping since $y^* = y^+$ for a ZPG boundary layer.

3.3.2. *SEP*

From the case with separation (SEP), three positions will be investigated. The positions are taken from the separated region ($x = 300$), at the reattachment point ($x = 412$), and in the recovery region ($x = 450$). The profiles are presented as functions of y^+ at all positions. Observe that the friction velocity is defined from (1) and (10), so it is everywhere positive.

At $x = 300$ the boundary layer is separated. At this position the non-linear term in the model expression for a_{12} does not give the same strong contribution to the distribution of a_{12} as in the APG1 case (see figure 6a).

The difference between the "W&J" and "Gir" models is supressed at this position where the boundary layer is separated, as seen from figure 6a.

The near-wall behaviour is entirely different from an attached layer. The non-damped profiles reach up to a positive value of 0.3 at the wall, due to that S_{12} is negative in a separated case. S_{12} at $x = 300$ is shown in figure 9a as the solid line. The two other profiles are the S_{12} for $x = 412$ and $x = 450$. Both in the APG1 case and in the SEP case in the attached region ($x = 450$), the non-damped profiles reach a value of -0.3 at the wall, because S_{12} is positive at those positions.

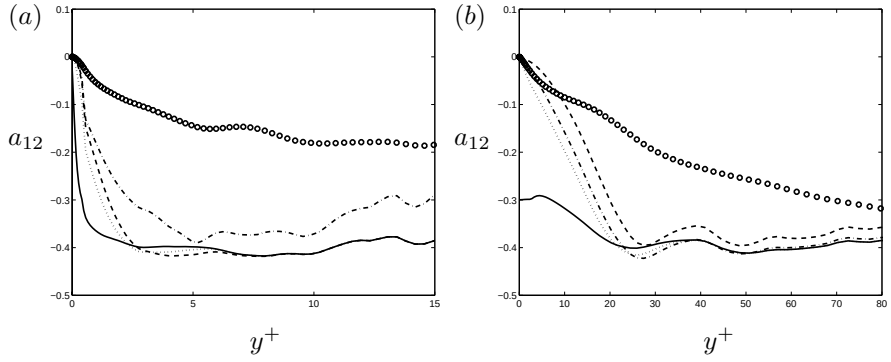

FIGURE 7. SEP at (a) $x = 412$. (b) $x = 450$. ∘ DNS; — non-damped "W&J". Damped "W&J" with the scaled coordinate in f_1 as - - y^*; $\cdots$ y^T; -·- y^+.

The damped "W&J" model at $x = 300$ is shown in figure 6b. Since the pressure gradient is more severe in this case (SEP), we do not expect the same value of A^+ to give the good agreement as for APG1 (remember that A^+ depends strongly on u_p/u_τ). Actually, the value of $A^+ = 26$ (solid line) gives better agreement than $A^+ = 11$ (dash-dotted line) in this case, as seen in figure 6b.

When using y^T in the expression for f_1, no much difference from the case of y^+ together with $A^+ = 11$ can be detected, see figure 6b. The y^* damping (dashed line in figure 6b) gives a better agreement near the wall. This is due to that y^* is zero close to the wall where the back-flow occurs, see equation (12).

At $x = 412$ the boundary layer is at its reattachment point. The DNS data and profiles from the EARSM are shown in figure 7a. At this position the non-damped profile from the "W&J" model stretches up to zero instead of approaching a constant value at the wall. This is due to that S_{12} goes to zero at the wall (zero wall shear stress). S_{12} at $x = 412$ is shown in figure 9a as the dashed line. Note that the boundary layer is much thinner in the viscous scaling at $x = 412$ due to the low value of u_τ at reattachment.

It is interesting to note in the DNS data that a_{12} is negative also in the separation bubble where S_{12} is negative. That means that an effective eddy viscosity is actually negative, which an algebraic model cannot reproduce. This effect is probably due to transport of the anisotropy in the thin near-wall layer.

At $x = 450$ the boundary layer is attached, and the near-wall behaviour is the same for as for APG1. The value of -0.3 is obtained with the non-damped "W&J" model, shown with the solid line in figure 7b. There is not much difference between the three different versions of the damping function, shown in figure 7b. The value $A^+ = 26$ was used for the damped model predictions in figures 7a and b. However, the damping is insensitive to the the value of A^+ at both positions $x = 450$ and $x = 412$. The damping is insufficient for

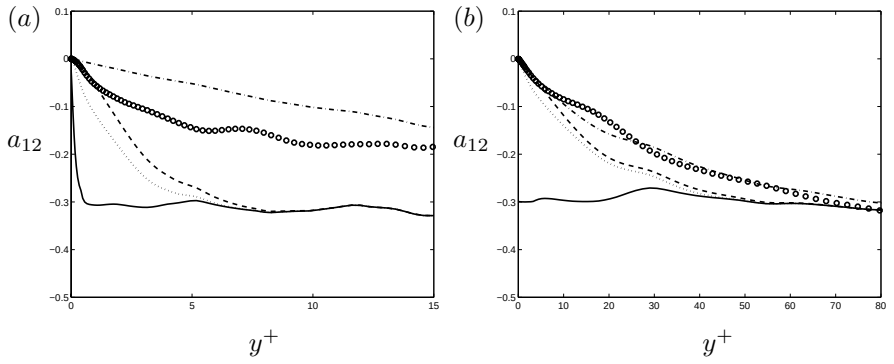

FIGURE 8. $a_{12} = f_1\beta_1 S_{12}$. SEP at (a) $x = 412$. (b) $x = 450$. $\circ$ DNS; — undamped "W&J" ($f_1 = 1$). Damped "W&J" with the scaled coordinate in f_1 as - - y^*; $\cdots$ y^T; -·- y^+.

all versions of f_1, and the reason is that the non-linear terms have influence in this region.

The general near-wall behaviour is the same for both positions $x = 450$ and $x = 412$, except for the important fact that also the non-damped profile at the wall is zero at $x = 412$, due to that the boundary layer is at its reattachment point. Even though the non-damped profiles are 'naturally' damped due to the value of zero at the wall, the damping works just as bad as for the position $x = 450$.

Thus, at both positions $x = 450$ and $x = 412$ (figures 7a and b), it is observed that the damping does not work very well. However, since the equation (14) is dependent on both the linear and non-linear terms, the effect of the damping is complicated. To isolate the effect of the damping of the linear term, only the first part of the expression for a_{12} is shown in figure 8a and b. The damping works very well on the linear part, especially for the position where the boundary layer is attached, figure 8b. The damping based on y^* or y^T gives as good agreement as y^+.

The different versions of the function f_1 (20, 29, 30) are shown at two downstream positions in figure 9b. The formulation with y^+ yields very different shapes at the two positions, whereas y^* and y^T give profiles close to each other. Note that f_1 based on y^* is zero up to $y^+ = 1$ at $x = 412$.

The damping functions at $x = 412$ are shown in figure 10a. The function based on y^+ increases very slowly while the functions based on y^* and y^T reach unity after approximately $y^+ = 8$. In figure 10b, the scaled normal coordinates are shown as a function of y^+. The largest difference between the three coordinates are found at this position where reattachment occurs ($x = 412$).

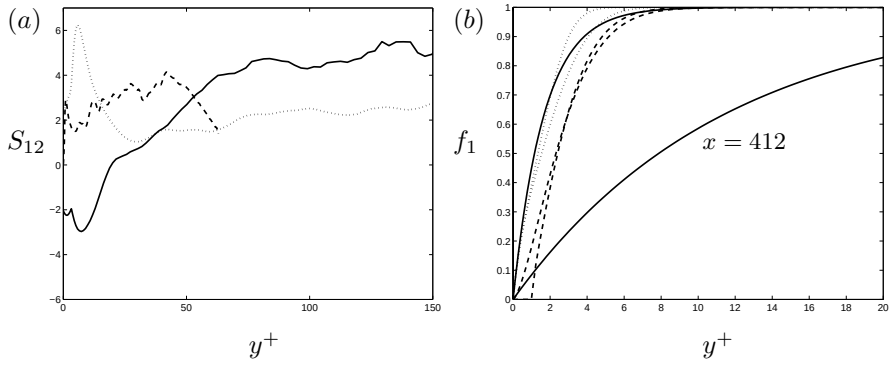

FIGURE 9. SEP: (a) S_{12} at — $x = 300$; - - $x = 412$; $\cdots$ $x = 450$. (b) f_1 at $x = 412$ and $x = 300$, using — y^+; - - y^*; $\cdots$ y^T.

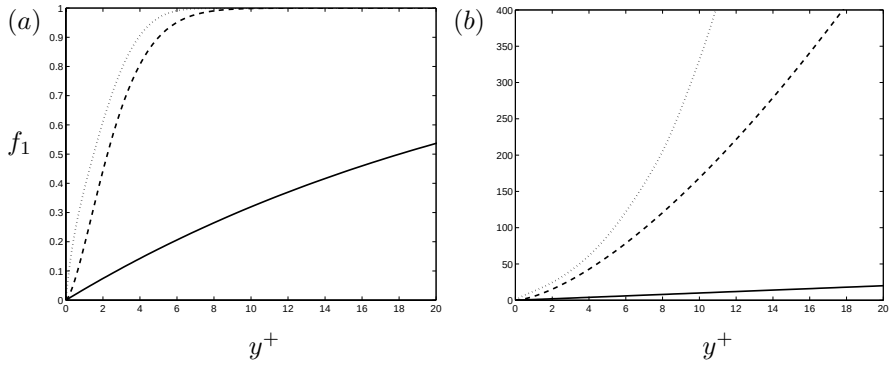

FIGURE 10. SEP at $x = 412$: (a) — y^+; - - y^*; $\cdots$ y^T. (b) f_1 using — y^+; - - y^*; $\cdots$ y^T.

3.4. *Similarities between the y^* and y^T scalings*

Let us try to analyze why the y^* and y^T scalings behave similar. The y^T relation is written in terms of Re_y according to (28). The dominating term, at least for small Re_y, is the $\sqrt{Re_y}$ term so essentially $y^T \sim \sqrt{Re_y}$. The $\sqrt{Re_y}$ term is simply motivated by that $Re_y \sim y^2$ since $K \sim y^2$ and the wanted behaviour is $y^T \sim y$ in the very near-wall region (the viscous sub-layer).

In the log region of the boundary layer there is another relation between Re_y and the y^* scaling that may be derived from the following. Let us first rewrite Re_y by using that $\langle u'v' \rangle = Ka_{12}$ as

$$Re_y \equiv \frac{y\sqrt{K}}{\nu} = y^+\sqrt{K^+} = \frac{1}{\sqrt{-a_{12}}} y^+ \sqrt{-\langle u'v' \rangle^+} \tag{31}$$

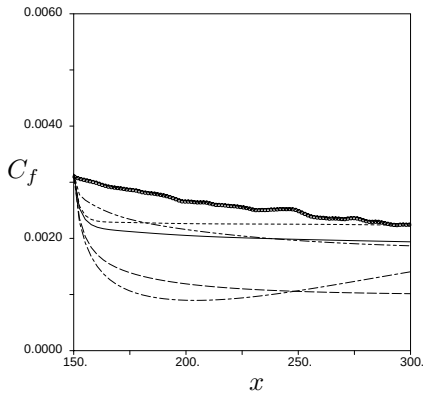

FIGURE 11. Computed skin friction coefficient C_f of the flat plate APG1 boundary layer compared to DNS data: — W&J EARSM with y^T damping; – – W&J EARSM with y^+ damping; - - - Girimaji EARSM with y^T damping; – - – Chien $K-\varepsilon$; – - - – Hanjalić RST.

Away from the viscous sub-layer, the viscosity may be neglected and then $-\langle u'v'\rangle^+ \approx 1 + (u_p/u_\tau)^3 y^+$ (see equation 5). By using the relation (9) the Reynolds number may be related to y^* as

$$Re_y \approx \frac{1}{\sqrt{-a_{12}}}\sqrt{(y^+)^2 + \left(\frac{u_p}{u_\tau}\right)^3 (y^+)^3} = \frac{y^*}{\sqrt{-a_{12}}} \tag{32}$$

Since a_{12} is rather constant (and independent of the pressure gradient) away from the wall there is a linear relation $Re_y \sim y^*$ in the log layer and Re_t and y^* could be expected to respond similarly to pressure gradients.

However, the leading order term in the y^T scaling is proportional to $\sqrt{Re_y}$ and, thus, $y^T \sim \sqrt{y^*}$. The $\sqrt{Re_y}$ dependency is adopted considering the viscous sub-layer where the assumption of neglected viscosity in (32) is basically wrong. This analysis, thus, only gives a qualitative explanation of the relation between y^* and y^T but gives an idea of why the two scalings behave similarly.

3.5. *Performance of the EARSM model*

The APG1 boundary layer was computed with a boundary layer solver using different turbulence models. The DNS data at $x = 150$ were used as inflow condition to the boundary layer computations.

The turbulence models tested are the Wallin & Johansson (2000) EARSM with the wall-damping function based both on y^+ and y^T, the corresponding EARSM based on the linearized SSG model (Girimaji 1997) with the Wallin & Johansson wall-damping function based on y^T, the Chien (1982) eddy-viscosity $K-\varepsilon$ model, and the Hanjalić *et al.* (1995) RST model. All three EARSMs are solved together with the Wilcox (1994) low-Reynolds number $K-\omega$ model.

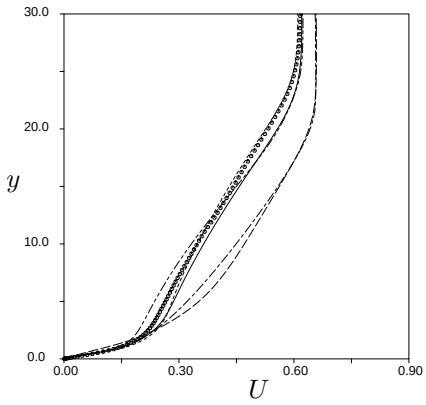

FIGURE 12. Computed mean velocity profiles at $x = 350$ for APG1 compared to DNS data. ∘ DNS data; — W&J EARSM with y^T damping; – – W&J EARSM with y^+ damping; - - - Girimaji EARSM with y^T damping; – - – Chien $K-\varepsilon$; – - - – Hanjalić RST.

Figure 11 shows the computed skin friction coefficient compared with DNS data. After an initial transient the computed skin friction levels out to some asymptotic behaviour. The transient is caused by inconsistency between the inflow data and the turbulence model. In the computations the coefficient $\beta \equiv \frac{\delta^*}{\tau_w}\frac{dP}{dx}$ was kept constant which leads to a reduced effect of the transient. Even though, the extent of the transient is rather large since the Reynolds number is relatively low. Computations with a given pressure gradient resulted in a separated flow for the y^+ based models, which will not be reported here.

There are two models that significantly deviates from the other models. These are the Chien $K-\varepsilon$ and the Wallin & Johansson EARSM with the wall-damping function based on y^+. The wall-damping function in the Chien model is also based on y^+. The other models do not use wall-damping functions based on y^+ and it is a reasonable assumption that the y^+ scaling is the major cause of the deviations. That is clearly seen if one compares the two computations using the Wallin & Johansson EARSM where the only difference between these two is the wall length scaling (y^+ or y^T).

Figure 12 shows the computed velocity profile compared with DNS data. Also here it is observed that the models with y^+ based near-wall damping compares bad with the DNS data while the other models are reasonably accurate. Also here one can notice the difference between the two computations using the Wallin & Johansson EARSM.

4. Conclusion

The viscous sub-layer in the near-wall boundary layer is largely governed by transport and non-equilibrium phenomena, which, in principle, only can be

captured by full Reynolds stress models. Eddy-viscosity models as well as algebraic Reynolds stress models must, thus, be modified by more or less empirical near-wall damping functions in order to have the correct near-wall asymptotic behaviour.

Near-wall damping functions based on y^+ become singular in separation or reattachment points and it was shown that the y^+ scaling also behaves badly in attached boundary layers with adverse pressure gradients. An alternative to y^+ was suggested by Wallin & Johansson (2000) and is basically $y^T \sim \sqrt{Re_y}$ where $Re_y \equiv y u_\tau / \nu$. It was found by use of the DNS data (APG1 and SEP) that the y^T scaling is reasonably similar to the pressure-gradient corrected analytical scaling y^* even close to separation.

In a general three-dimensional CFD method the formulation in terms of y^T is more attractive since that can be derived in every grid point by using local field variables and the wall distance. The use of Y^* involves the skin friction of the nearest wall and also the local pressure gradient. Moreover, in general three-dimensional cases the skin friction, pressure gradient, and external flow are not in general aligned which introduces additional complications.

When damping the a_{12} component of the anisotropy with a van Driest type of wall damping function it was found that the model predictions were much improved by using y^T or y^* compared to y^+ but there was still a significant deviation from the DNS data for the APG1 case. It is obvious that there are other aspects of damping the a_{12} anisotropy in adverse pressure gradients than the wall distance scaling which could not be resolved within this study.

Comparisons between the Wallin & Johansson EARSM based on a LRR-type of pressure-strain model and the Girimaji EARSM which is based on the linearized SSG show no major differences. The only significant difference is that the a_{33} anisotropy component is non-zero for the Girimaji model whereas it is zero for the Wallin & Johansson model away from the viscous sub-layer. However, the deviation from the DNS data is about the same for both models.

References

Cebeci, T. 1970 Behavior of turbulent flow near a porous wall with pressure gradient. *AIAA J.* **8** (12), 2152–2156.

Cebeci, T. & Smith, A. M. O. 1968 A finite-difference solution of the incompressible turbulent boundary-layer equations by an eddy-viscosity concept. 1968 AFOSR-IFP-Stanford Conference. Vol 1.

Chien, K. Y. 1982 Predictions of channel and boundary-layer flows with a low-Reynolds-number turbulence model. *AIAA J.* **20**, 33–38.

Girimaji, S. S. 1997 A Galilean invariant explicit algebraic reynolds stress model for turbulent curved flows. *Phys. Fluids* **9**, 1067–1077, (Also ICASE Report No. 96-38).

Granville, P. S. 1989 A modified van driest formula for the mixing length of turbulent boundary layers in pressure gradients. *J. Fluids Eng.* **111**, 94–97.

Hanjalić, K., Jakirlić, S. & Hadžić, I. 1995 Computation of oscillating turbulent flows at transitional *Re*-numbers. In *Turbulent Shear Flows 9* (eds. F. Durst, N. Kasagi & B. E. Launder), pp. 323–342. Springer-Verlag.

Kays, W. M. 1971 Heat transfer to the transpired boundary layer. ASME Paper No. 71-HT-44.

Launder, B. E., Reece, G. J. & Rodi, W. 1975 Progress in the development of a Reynolds-stress turbulence closure. *J. Fluid Mech.* **68**, 537 – 566.

McDonald, H. 1969 The effect of pressure gradient on the law of the wall in turbulent flow. *J. Fluid Mech.* **35**, 311–336.

Nagano, Y., Tagawa, M. & Tsuji, T. 1992 Effects of adverse pressure gradients on mean flows and turbulence statistics in a boundary layer. In *Turbulent Shear Flows 8* (eds. F. Durst, R. Friedrich, B. E. Launder, F. W. Schmitd, U. Schumann & J. H. Whitelaw), pp. 7–21. Springer-Verlag.

Perry, A. E., Bell, J. B. & Joubert, P. N. 1966 Velocity and temperature profiles in adverse pressure gradient turbulent boundary layers. *J. Fluid Mech.* **25**, 299–320.

Skåre, P. E. & Krogstad, P.-Å. 1994 A turbulent equilibrium boundary layer near separation. *J. Fluid Mech.* **272**, 319–348.

Skote, M., Henkes, R. A. W. M. & Henningson, D. S. 1998 Direct numerical simulation of self-similar turbulent boundary layers in adverse pressure gradients. *Flow, Turbulence and Combustion* **60**, 47–85.

Skote, M. & Henningson, D. 1999 Analysis of the data base from a dns of a separating turbulent boundary layer. Center for Turbulence Research, Annual Research Briefs 1999, 225–237.

Skote, M. & Henningson, D. S. 2000 Direct numerical simulation of a separating turbulent boundary layer. *J. Fluid Mech.* (Submitted).

Speziale, C. G., Sarkar, S. & Gatski, T. B. 1991 Modelling the pressure–strain correlation of turbulence: an invariant dynamical systems approach. *J. Fluid Mech.* **227**, 245–272.

Stratford, B. S. 1959 The prediction of separation of the turbulent boundary layer. *J. Fluid Mech.* **5**, 1–16.

Tennekes, H. & Lumley, J. L. 1972 *A First Course in Turbulence*. The MIT Press.

Townsend, A. A. 1961 Equilibrium layers and wall turbulence. *J. Fluid Mech.* **11**, 97–120.

Wallin, S. & Johansson, A. V. 2000 An explicit algebraic Reynolds stress model for incompressible and compressible turbulent flows. *J. Fluid Mech.* **403**, 89–132.

Wilcox, D. C. 1993 *Turbulence Modeling for CFD*. DCW Industries, Inc.

Wilcox, D. C. 1994 Simulation of transition with a two-equation turbulence model. *AIAA J.* **32**, 247–255.